International Journal of Heat and Mass Transfer 137 (2019) 1053–1063

Contents lists available at ScienceDirect

International Journal of Heat and Mass Transfer

journal homepage: www.elsevier.com/locate/ijhmt

Full-spectrum correlated-*k*-distribution look-up table for radiative transfer in nonhomogeneous participating media with gas-particle mixtures

Chaojun Wang [a], Boshu He [a,b,*], Michael F. Modest [c]

[a] Institute of Combustion and Thermal Systems, School of Mechanical, Electronic and Control Engineering, Beijing Jiaotong University, Beijing 100044, People's Republic of China
[b] School of Mechanical and Power Engineering, Haibin College of Beijing Jiaotong University, Huanghua 061199, Hebei Province, People's Republic of China
[c] School of Engineering, University of California, Merced 95340, USA

ARTICLE INFO

Article history:
Received 2 February 2019
Received in revised form 25 March 2019
Accepted 25 March 2019
Available online xxxx

Keywords:
Radiative heat transfer
Full-spectrum correlated-*k*-distribution (FSCK)
Look-up table
Nonhomogeneous particulate media
Gas-particle mixtures

ABSTRACT

The full-spectrum correlated-*k*-distribution (FSCK) look-up table previously developed by the authors Wang et al. (2018) provides an efficient means for accurate calculations of radiative properties of gas-soot mixtures. Except for those of soot, radiative properties of particles are impossible to tabulate in FSCK look-up tables since particles of different compositions and sizes may have different local temperatures. In order to combine the radiative properties of particles with those of gas-soot mixtures from the FSCK look-up table, two schemes named gas FSK-particle FSK (FSK-FSK) and gas FSK-particle Gray (FSK-Gray) schemes, are proposed. The FSK-FSK scheme employs the correlation principle to obtain the radiative properties of gas-particle mixtures in FSCK form on-the-fly while the FSK-Gray scheme uses the Planck-mean absorption coefficient to represent particle spectral behavior. Several radiative heat transfer calculations across a 1D slab are carried out to test the accuracy of the two schemes. Furthermore, radiative heat transfer in a realistic coal flame and a scaled version of it are determined to validate the performance of the developed scheme. Results show that use of either scheme gives results of excellent accuracy with extremely low computational cost compared to benchmark line-by-line results.

1. Introduction

Due to its dependence on the fourth power in temperature, radiative heat transfer is the dominant heat transfer mode during combustion of solid fuels, e.g., pulverized or fluidized bed coal combustion [1–7]. Therefore, a high-fidelity radiation model accounting for radiative contributions from both gas phase and particulate phase is of great importance for in-depth insight of solid combustion simulations. This leads to the need of accurate characterization of radiative properties for both gases and particles.

Radiative properties of gases, mainly CO_2, H_2O and CO, display very strong spectral or 'nongray' behavior across the spectrum in high-temperature environments [8,9]. The most accurate models for radiative properties are the so-called line-by-line (LBL) calculations [10], which require absorption coefficients at over one million wavenumbers and, therefore, make them prohibitive in practical simulations because of the huge computational power required. An excellent alternative model named full-spectrum *k*-distribution (FSK) method was proposed by Modest [11] based on the reordering concept. With spectral integration performed using *k*-distributions across an artificial spectrum, the FSK method can reduce the number of radiative transfer equation (RTE) evaluations from over one million to around ten without losing accuracy. To avoid the cumbersome processes of both assembling and mixing *k*-distributions, Wang et al. [12] constructed an FSK look-up table that can be applied in nonhomogeneous gaseous media over a large range of thermodynamic states, and can achieve near LBL accuracy, but at a tiny fraction of the LBL computational cost.

As an intermediate particulate species during most combustion scenarios, soot plays a very important role in radiation [13,14]. Since soot particles are very small, they are generally at the same temperature as the flame, which means the *k*-distributions of soot can be weighted by the same Planck function as those of gases. Moreover, the most commonly used correlations for calculations of radiative properties of soot [15] are linearized with soot volume fraction. This allows radiative properties of soot to be included in

* Corresponding author at: Institute of Combustion and Thermal Systems, School of Mechanical, Electronic and Control Engineering, Beijing Jiaotong University, Beijing 100044, People's Republic of China.
E-mail address: hebs@bjtu.edu.cn (B. He).

https://doi.org/10.1016/j.ijheatmasstransfer.2019.03.149
0017-9310/

Nomenclature

a	nongray stretching function in FSK method, –
f	full-spectrum k-distribution, m
f_v	volume fraction, –
f_A	projected area per unit volume, m^{-1}
g	cumulative full-spectrum k-distribution, –
I	radiative intensity, $W/(m^2\ sr)$
k	absorption coefficient variable, m^{-1}
m	complex index of refraction, $m = n - ik$
p	total pressure, bar
q	radiative heat flux, W/m^2
T	temperature, K
$\hat{\boldsymbol{s}}$	direction vector, –
r	radial length, m
V	cell volume, m^3
x	mole fraction, –
z	axial length, m

Greek symbols

$\delta(\cdot)$	Dirac-Delta function, –
ϕ	vector of local thermodynamic state variables, –
η	wavenumber, m^{-1}
κ_η	spectral absorption coefficient, m^{-1}
κ_P	Planck-mean absorption coefficient, m^{-1}
σ	Stefan-Boltzmann constant, $5.67 \times 10^{-8}\ W/(m^2 \cdot K^4)$
σ_s	scattering coefficient, m^{-1}
Φ	scattering phase function, –
Ω	solid angle, sr

Subscripts

b	blackbody
C	cell-based

Superscripts

0	reference state

Abbreviations

FSK	full-spectrum k-distribution
FSCK	full-spectrum correlated-k-distribution
LBL	line-by-line
RTE	radiative transfer equation
WSGG	weighted sum of gray gases

the FSK look-up table together with those of gases using the same Planck function. The relevant work was done by Wang et al. [16,17] and, more recently, they developed an updated full-spectrum correlated-k-distribution (FSCK) look-up table [18] including CO_2, H_2O, CO and soot, which provides a more efficient alternative to calculate the radiative properties of gas-soot mixtures.

Other types of important particles are the relatively large coal and fly ash particles formed during combustion. Different from soot, these particles may not have the same temperature as the flame. Therefore, accurate description of the radiative properties of multi-phase mixtures with different temperatures for each phase using the FSK method is impossible, since the k-distributions of these particles cannot be weighted by the same Planck function as those of gases. In addition, the correlations used for the calculations of radiative properties of particles, e.g., the correlations proposed by Buckius and Hwang [19] or Mengüç and Viskanta [20], are nonlinear with particle size, complex index of refraction and irradiating wavelength. Consequently, tabulation of radiative properties based on the FSK method for gas-particle mixtures in different local temperatures becomes a Herculean task.

Considering the outstanding advantages of the FSK method, combining the radiative properties of gases and particles using the FSK method is attractive and desirable, but only a few attempts have been made, and it remains difficult to achieve good performance in both accuracy and efficiency for the predictions of radiative properties of gas-particle mixtures using the FSK method. For example, Cai et al. [21] proposed an absorption coefficient regression scheme to determine 'effective' k-values across a narrow-band and then directly added them to the gas k-distributions of that narrow-band. While near LBL accuracy can be achieved, use of the regression scheme is time-consuming due to cumbersome assembly. Another example was given by Guo et al. [22,23] who combined the features of the FSK method with the weighted sum of gray gases (WSGG) method to calculate radiative properties for fly ash without increasing computational complexity. However, relative errors for the radiative heat source in their work were as high as 15% compared to the LBL solution.

To overcome this dilemma, two schemes are proposed to combine the radiative properties of particles with those of gas-soot mixtures from the FSCK look-up table. Employing both schemes, radiative properties of gas-particle mixtures can be directly obtained by combining the particulate part from on-the-fly calculations with the gas-soot part from the FSCK look-up table. Radiative calculations for 1D slabs and a realistic coal flame were carried out to test the performance of the two schemes, demonstrating their validity in both accuracy and efficiency.

2. Theoretical background

2.1. Full-spectrum correlated-k-distribution

A full-spectrum k-distribution is a reordered absorption coefficient that accounts for the variation of the Planck function and is defined as [24]

$$f_{T,\phi}(k) = \frac{1}{I_b(T)} \int_0^\infty I_{b\eta}(T)\delta(k - \kappa_\eta(\boldsymbol{\phi}))\mathrm{d}\eta \tag{1}$$

where κ_η is the spectral absorption coefficient calculated from a spectroscopic database; k is the nominal absorption coefficient variable, which has the same range as κ_η; $\delta(\cdot)$ is the Dirac-Delta function; $\boldsymbol{\phi}$ is a vector of thermodynamic state variables for gas-soot mixtures including pressure, temperature and species concentration; $f_{T,\phi}(k)$ is a Planck-function-weighted k-distribution with absorption coefficient evaluated at the local state $\boldsymbol{\phi}$ and a Planck function temperature T; I_b and $I_{b\eta}$ are the Planck function and the spectral Planck function, respectively; η is the wavenumber.

The cumulative full-spectrum k-distribution is defined as

$$g_{T,\phi}(k) = \int_0^k f_{T,\phi}(k')\mathrm{d}k' \tag{2}$$

Thus, g represents the fraction of the spectrum whose absorption coefficient lies below the value of k and, therefore, $0 \leqslant g \leqslant 1$. Inverting Eq. (2), a smooth, monotonically increasing function, $k_{T,\phi}(g)$, can be obtained, with minimum and maximum values identical to those of the absorption coefficients.

To apply the FSK method to a nonhomogeneous mixture, radiative properties need to be transformed into a unified reference g-space (g^0), which is usually achieved by employing the correlation principle as follows

$$g_{T,\phi^0}(k) = g_{T,\phi}(k^*) \tag{3}$$

and the FSK based on Eq. (3) is the so-called full-spectrum correlated-k-distribution (FSCK) method.

2.2. Multiphase radiative transfer equation

The multiphase RTE includes terms for both the gas phase and the particulate phase. Consider a gas-particle mixture with particles grouped into N different phases according to their material and/or sizes with $i = 1, 2, \ldots, N$ and, in particular, let $i = 0$ be the gas-soot mixture since it is at the same temperature during combustion. Therefore, particles in the following context refer to those excluding soot. Particles of different sizes possess different radiative properties and may have different temperatures due to different reaction rates and responses to heat transfer. The spectral RTE at wavenumber η including absorption, scattering and multiple temperature emission for a gas-particle mixture may be stated as [24]

$$\frac{\mathrm{d}I_\eta}{\mathrm{d}s} = \sum_{i=0}^{N} \kappa_{\eta,i} I_{b\eta}(T_i) - \sum_{i=0}^{N} \kappa_{\eta,i} I_\eta - \sum_{i=1}^{N} \sigma_{s,i} I_\eta + \sum_{i=1}^{N} \frac{\sigma_{s,i}}{4\pi} \times \int_{4\pi} I_\eta(\hat{\boldsymbol{s}}') \Phi_i(\hat{\boldsymbol{s}}, \hat{\boldsymbol{s}}') \mathrm{d}\Omega \tag{4}$$

where scattering from the gas-soot mixture is neglected and the scattering coefficient σ_s as well as the phase function Φ are assumed to be gray. This treatment follows the work of Modest and Riazzi [25] who demonstrated that gray scattering coefficients and phase functions are valid approximations even for extremely nongray scatters. In this work, the spectral absorption coefficients are obtained from a LBL database [26] for gas (updated to HITEMP2010 [27]) and correlations [15] for soot; for coal and fly ash particles, the radiative properties are calculated using correlations proposed by Buckius and Hwang [19]. Since the soot correlation employs a spectrally varying index of refraction, it is nonlinearly dependent on spectral variable, the soot absorption coefficients used here are nongray and not linearly proportional to the spectral variable. The Buckius-Hwang correlations present spectral correlations for the absorption coefficient of particles in terms of the complex index of refraction and the size parameter. Here, a constant complex index of refraction is assumed for each particulate phase, hence the spectral dependence of the complex index of refraction for particles is neglected. However, particles are still nongray due to their spectrally-dependent size parameters.

3. Combination of radiative properties for gas-particle mixtures

In principle, the radiative properties of gas-particle mixtures can be combined on the spectral level as given by Eq. (4) as long as LBL calculations are carried out at many wavenumbers. Because of the huge computational cost, this scheme referred to as the gas LBL-particle LBL or the LBL-LBL scheme is only used for benchmark solutions in this work.

During combustion, particles may have different temperatures than the gas and, therefore, the reordering process given by Eq. (1) cannot be carried out with a single Planck function. The only way to obtain radiative properties of gas-particle mixtures in the FSK form appears to be directly mixing the individual k-distributions of gas and those of particles. While some mixing schemes have been proposed, e.g., the multiplication scheme [28] and the uncorrelated scheme [25], they are only valid for gases. In the following, details are developed how to add individual k-distributions of particles to those of gas-soot mixtures from the FSCK look-up table, which will be referred to as the gas FSK-particle FSK or the FSK-FSK scheme. In addition, a simpler method using radiative properties from the FSCK look-up table together with gray particles is also given, which is referred to as the gas FSK-particle Gray or the FSK-Gray scheme.

3.1. FSK-FSK scheme

The FSK method is generally based on reordering of mixture absorption coefficients that share the same thermodynamic state. This causes a problem for gas-particle mixtures since they may possess different temperatures during combustion, for which the absorption coefficients $\kappa_{\eta,i}$ in the emission term, i.e., first term on the right hand of Eq. (4), cannot be simply added up. On the other hand, an inspection of the spectral distribution of absorption coefficients for both gases and particles, shown in Fig. 1, reveals that the spectral complexities are mostly due to the gas phase. Since the purpose of reordering is to simplify spectral complexities, reordering will be done for the absorption coefficients of gas-soot mixtures only. In nonhomogeneous media, this is achieved by multiplying the RTE with the Dirac-Delta function and then integrating over the full spectral range:

$$\int_0^\infty [\cdot]\delta(k_0(\boldsymbol{\phi}^0) - \kappa_{\eta,0}(\boldsymbol{\phi}^0))\mathrm{d}\eta \tag{5}$$

where $\boldsymbol{\phi}^0$ represents a reference state of gas-soot mixtures and k_0 is equivalent to $\kappa_{\eta,0}$ at $\boldsymbol{\phi}^0$. Each term in Eq. (4) can then be reordered as follows:

(1) Intensity gradient

$$\int_0^\infty \frac{\mathrm{d}I_\eta}{\mathrm{d}s}\delta(k_0(\boldsymbol{\phi}^0) - \kappa_{\eta,0}(\boldsymbol{\phi}^0))d\eta = \frac{\mathrm{d}}{\mathrm{d}s}\int_0^\infty I_\eta\delta(k_0(\boldsymbol{\phi}^0) - \kappa_{\eta,0}(\boldsymbol{\phi}^0))d\eta = \frac{\mathrm{d}I_k}{\mathrm{d}s} \tag{6}$$

where

$$I_k = \int_0^\infty I_\eta\delta(k_0(\boldsymbol{\phi}^0) - \kappa_{\eta,0}(\boldsymbol{\phi}^0))d\eta \tag{7}$$

(2) Emission

$$\begin{aligned} &\int_0^\infty \left(\sum_{i=0}^N \kappa_{\eta,i} I_{b\eta}(T_i)\right)\delta(k_0(\boldsymbol{\phi}^0) - \kappa_{\eta,0}(\boldsymbol{\phi}^0))d\eta \\ &= \sum_{i=0}^N \int_0^\infty \kappa_{\eta,i}(\boldsymbol{\phi}_i) I_{b\eta}(T_i)\delta(k_0(\boldsymbol{\phi}^0) - \kappa_{\eta,0}(\boldsymbol{\phi}^0))d\eta \\ &\cong \sum_{i=0}^N k_i^*(\boldsymbol{\phi}_i)\int_0^\infty I_{b\eta}(T_i)\delta(k_0(\boldsymbol{\phi}^0) - \kappa_{\eta,0}(\boldsymbol{\phi}^0))d\eta \\ &= \sum_{i=0}^N k_i^*(\boldsymbol{\phi}_i) f_{T_i,\phi^0}(k_0) I_b(T_i) \end{aligned} \tag{8}$$

where k_i^* represents a correlated k-value for phase i and $\boldsymbol{\phi}_i$ ($i \geqslant 1$) is a vector of state variables for particles including particle temperature, size and volume fraction. The approximation made in the third line is due to employment of the correlation principle, assuming the absorption coefficient of the gas-soot mixture at the reference state $\boldsymbol{\phi}^0$ to be correlated with absorption coefficients for both gas-soot mixtures and particles at their local state $\boldsymbol{\phi}_i$. In practical applications, this correlation is always violated to some degree and may become a major source of error.

(3) Absorption

$$\begin{aligned} &-\int_0^\infty \left(\sum_{i=0}^N \kappa_{\eta,i} I_\eta\right)\delta(k_0(\boldsymbol{\phi}^0) - \kappa_{\eta,0}(\boldsymbol{\phi}^0))\mathrm{d}\eta \\ &= -\sum_{i=0}^N \int_0^\infty \kappa_{\eta,i}(\boldsymbol{\phi}_i) I_\eta\delta(k_0(\boldsymbol{\phi}^0) - \kappa_{\eta,0}(\boldsymbol{\phi}^0))\mathrm{d}\eta \\ &\cong -\sum_{i=0}^N k_i^*(\boldsymbol{\phi}_i)\int_0^\infty I_\eta\delta(k_0(\boldsymbol{\phi}^0) - \kappa_{\eta,0}(\boldsymbol{\phi}^0))\mathrm{d}\eta \\ &= -\sum_{i=0}^N k_i^*(\boldsymbol{\phi}_i) I_k \end{aligned} \tag{9}$$

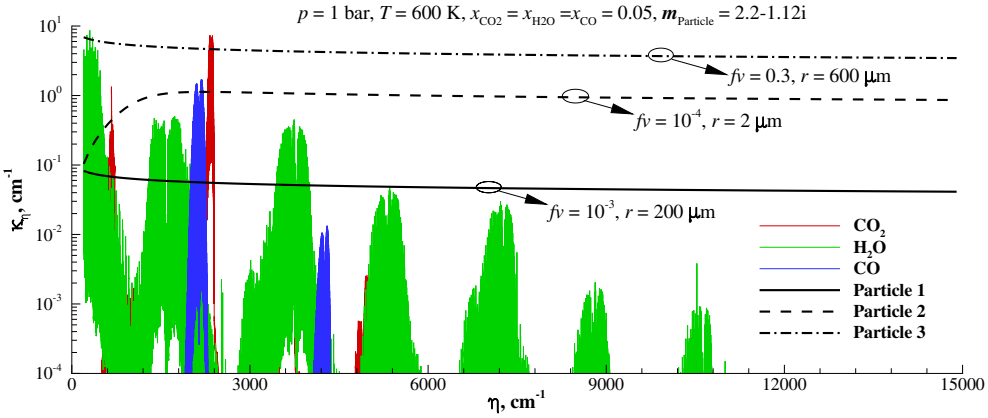

Fig. 1. Spectral absorption coefficients of CO_2, H_2O and CO in nitrogen as well as typical particles across spectrum.

where the correlated principle employed in the derivation of the emission term is also used here.

(4) Scattering

$$\begin{aligned}&\int_0^\infty\left(-\sum_{i=0}^N\sigma_{s,i}I_\eta+\sum_{i=0}^N\tfrac{\sigma_{s,i}}{4\pi}\int_{4\pi}I_\eta(\hat{s}')\Phi_i(\hat{\boldsymbol{s}},\hat{s}')\mathrm{d}\Omega\right)\delta\left(k_0(\boldsymbol{\phi}^0)-\kappa_{\eta,0}(\boldsymbol{\phi}^0)\right)\mathrm{d}\eta\\&=-\sum_{i=1}^N\int_0^\infty\sigma_{s,i}I_\eta\delta\left(k_0(\boldsymbol{\phi}^0)-\kappa_{\eta,0}(\boldsymbol{\phi}^0)\right)\mathrm{d}\eta\\&+\sum_{i=1}^N\tfrac{\sigma_{s,i}}{4\pi}\int_{4\pi}\int_0^\infty I_\eta(\hat{s}')\delta\left(k_0(\boldsymbol{\phi}^0)-\kappa_{\eta,0}(\boldsymbol{\phi}^0)\right)\mathrm{d}\eta\Phi_i(\hat{\boldsymbol{s}},\hat{\boldsymbol{s}}')\mathrm{d}\Omega\\&=-\sum_{i=1}^N\sigma_{s,i}I_k+\sum_{i=1}^N\tfrac{\sigma_{s,i}}{4\pi}\int_{4\pi}I_k(\hat{\boldsymbol{s}}')\Phi_i(\hat{\boldsymbol{s}},\hat{\boldsymbol{s}}')\mathrm{d}\Omega\end{aligned}\tag{10}$$

Combining the above terms, the reordered RTE becomes

$$\frac{\mathrm{d}I_k}{\mathrm{d}s}=\sum_{i=0}^N k_i^*(\boldsymbol{\phi}_i)f_{T_i,\boldsymbol{\phi}^0}(k_0)I_b(T_i)-\sum_{i=0}^N k_i^*(\boldsymbol{\phi}_i)I_k-\sum_{i=1}^N\sigma_{s,i}I_k+\sum_{i=1}^N\times\frac{\sigma_{s,i}}{4\pi}\int_{4\pi}I_k(\hat{\boldsymbol{s}}')\Phi_i(\hat{\boldsymbol{s}},\hat{\boldsymbol{s}}')\mathrm{d}\Omega\tag{11}$$

Dividing by the k-distribution at the reference state $\boldsymbol{\phi}^0$ of gas-soot mixtures, the multiphase RTE can be written in the FSCK form as

$$\frac{\mathrm{d}I_g}{\mathrm{d}s}=\sum_{i=0}^N k_i^*(g^0)a_{T_i,T^0}(g^0)I_b(T_i)-\sum_{i=0}^N k_i^*(g^0)I_g-\sum_{i=1}^N\sigma_{s,i}I_g+\sum_{i=1}^N\times\frac{\sigma_{s,i}}{4\pi}\int_{4\pi}I_g(\hat{\boldsymbol{s}}')\Phi_i(\hat{\boldsymbol{s}},\hat{\boldsymbol{s}}')\mathrm{d}\Omega\tag{12}$$

where g^0 represents the reference g-space, and

$$I_g=I_k/f_{T^0,\boldsymbol{\phi}^0}(k_0)=\frac{\int_0^\infty I_\eta\delta\left(k_0(\boldsymbol{\phi}^0)-\kappa_{\eta,0}(\boldsymbol{\phi}^0)\right)\mathrm{d}\eta}{f_{T^0,\boldsymbol{\phi}^0}(k_0)}\tag{13}$$

$$a_{T_i,T^0}(g^0)=\frac{f_{T_i,\boldsymbol{\phi}^0}(k_0)}{f_{T^0,\boldsymbol{\phi}^0}(k_0)}=\frac{\mathrm{d}g_{T_i,\boldsymbol{\phi}^0}(k_0)}{\mathrm{d}g_{T^0,\boldsymbol{\phi}^0}(k_0)}\tag{14}$$

In order to determine correlated k-values for gas-soot mixtures, i.e., $k_0^*(g^0)$ in Eq. (12), the latest implementation [18] is employed, the heart of which was to employ the correlation principle twice so that total emission is conserved. Based on this idea, the FSCK look-up table including CO_2, H_2O, CO and soot has been constructed, providing an accurate and efficient database for directly obtaining $k_0^*(g^0)$.

While there is no available database for correlated k-values of particles, i.e., $k_i^*(g^0)$ when $i\geqslant 1$ in Eq. (12), they can be calculated on-the-fly following the same idea. As a start, the employment of the correlation principle gives

$$g_{T^0,\boldsymbol{\phi}^0}=g_{T^0,\boldsymbol{\phi}_i}\tag{15}$$

which means the reference g-space is only related to the Planck function temperature regardless of the vector of state variables. This provides an approximate method to manipulate the correlated k-values of gas-soot mixtures and those of particles in the g-space determined by the reference temperature of gas-soot mixtures.

Since the k-distributions of particles always belong to the g-space determined by their local temperatures, it is required to map those k-distributions into the reference g-space. This can be achieved by employing two interpolations

$$k_{T^0,\boldsymbol{\phi}_i(T^0)}\left(g_{T^0,\boldsymbol{\phi}_i(T^0)}\right)\xrightarrow{\text{1st interpolation}}g_{T_i,\boldsymbol{\phi}_i(T^0)}\left(k_{T^0,\boldsymbol{\phi}_i(T^0)}\right)\xrightarrow{\text{2nd interpolation}}k_{T_i,\boldsymbol{\phi}_i(T_i)}\left(g_{T_i,\boldsymbol{\phi}_i(T^0)}\right)\tag{16}$$

where for clarity, the particle state $\boldsymbol{\phi}_i$ is written out here to show one of its sub-variables, i.e., particle temperature. This process of interpolations is analyzed in detail in [18] and briefly described here for completeness. The first interpolation is to find g-values on the $k_{T_i,\boldsymbol{\phi}_i(T^0)}\left(g_{T_i,\boldsymbol{\phi}_i(T^0)}\right)$ distribution according to k-values on the $k_{T^0,\boldsymbol{\phi}_i(T^0)}\left(g_{T^0,\boldsymbol{\phi}_i(T^0)}\right)$ distribution, which is theoretically accurate since the k-distributions of $k_{T_i,\boldsymbol{\phi}_i(T^0)}\left(g_{T_i,\boldsymbol{\phi}_i(T^0)}\right)$ and $k_{T^0,\boldsymbol{\phi}_i(T^0)}\left(g_{T^0,\boldsymbol{\phi}_i(T^0)}\right)$ share the same k-values. The second interpolation is to determine correlated k-values on $k_{T_i,\boldsymbol{\phi}_i(T_i)}\left(g_{T_i,\boldsymbol{\phi}_i(T_i)}\right)$ distribution (local k-distribution) according to the g-values found in the first interpolation. It should be noted that absorption coefficients of particles are independent of temperature when using constant and gray complex indices of refraction. This means $k_{T_i,\boldsymbol{\phi}_i(T_i)}\left(g_{T_i,\boldsymbol{\phi}_i(T_i)}\right)$ is exactly the same as $k_{T_i,\boldsymbol{\phi}_i(T^0)}\left(g_{T_i,\boldsymbol{\phi}_i(T^0)}\right)$ and, therefore, the second interpolation is theoretically accurate as well. Then, the correlated k-values of particles can be expressed as

$$k_i^*(g^0)=k_{T_i,\boldsymbol{\phi}_i(T_i)}\left(g_{T^0,\boldsymbol{\phi}_i(T^0)}\right)=k_{T_i,\boldsymbol{\phi}_i(T_i)}\left(g_{T_i,\boldsymbol{\phi}_i(T^0)}\right),\quad i\geqslant 1\tag{17}$$

where the second term is a full expression of $k_i^*(g^0)$ and the last term gives the expression of correlated k-values using the above interpolations.

Correspondingly, the a-values of particles using the correlation principle shown in Eq. (14) can be expressed as

$$a_{T_i,T^0}(g^0)=\frac{\mathrm{d}g_{T_i,\boldsymbol{\phi}_i}(k)}{\mathrm{d}g_{T^0,\boldsymbol{\phi}_i}(k)},\quad i\geqslant 1\tag{18}$$

Employing the above correlated k-values and the a-values, the total emission term for particles i can be written as

$$\begin{aligned}&\int_0^1 k_i^*(g^0)a_{T_i,T^0}(g^0)I_b(T_i)\mathrm{d}g^0\\&= I_b(T_i)\int_0^1 k_{T_i,\phi_i(T_i)}\left(g_{T_i,\phi_i(T^0)}\right)\frac{\mathrm{d}g_{T_i,\phi_i}(k)}{\mathrm{d}g_{T^0,\phi_i}(k)}\mathrm{d}g_{T^0,\phi_i}(k)\\&= I_b(T_i)\int_0^1 k_{T_i,\phi_i}\left(g_{T_i,\phi_i}\right)\mathrm{d}g_{T_i,\phi_i}(k)=\kappa_{P,i}(T_i)I_b(T_i),\quad i\geqslant 1\end{aligned}\tag{19}$$

where κ_P represents the Planck mean absorption coefficient and the total emission is conserved.

To sum up, the FSK-FSK calculations for particles require two raw particulate k-distributions, i.e., $k_{T^0,\phi_i(T^0)}\left(g_{T^0,\phi_i(T^0)}\right)$ and $k_{T_i,\phi_i(T^0)}\left(g_{T_i,\phi_i(T^0)}\right)$, two interpolations for correlated k-values and one additional interpolation for a-values. The raw particulate k-distributions are directly generated from the absorption coefficients of particles calculated on-the-fly. Due to the relatively gentle spectral behavior, the resolution for the absorption coefficients of particles is set to 100 cm^{-1}, at which LBL emission still provides high accuracy. This guarantees efficient on-the-fly calculations for obtaining correlated k-values for particles without any changes to the FSCK look-up table.

3.2. FSK-Gray scheme

Considering the fact that the absorption coefficients of particles display simple spectral behavior, as shown in Fig. 1, it is natural to carry out a straightforward FSK-Gray scheme that only takes into account of the spectral behavior for gas-soot mixtures using the FSK method and treats particles as gray. The RTE shown in Eq. (12) can then be simplified to

$$\begin{aligned}\frac{\mathrm{d}I_g}{\mathrm{d}s}=&k_0^*(g^0)a_{T_0,T^0}(g^0)I_b(T_0)-k_0^*(g^0)I_g+\sum_{i=1}^{N}\kappa_{P,i}I_b(T_i)\\&-\sum_{i=1}^{N}\kappa_{P,i}I_g-\sum_{i=1}^{N}\sigma_{s,i}I_g+\sum_{i=1}^{N}\frac{\sigma_{s,i}}{4\pi}\int_{4\pi}I_g(\hat{\boldsymbol{s}}')\Phi_i(\hat{\boldsymbol{s}},\hat{\boldsymbol{s}}')\mathrm{d}\Omega\end{aligned}\tag{20}$$

In FSK-Gray calculations, the correlated k-values of gas-soot mixtures are still obtained from the FSCK look-up table while the Planck mean absorption coefficients for particles are calculated on-the-fly using absorption coefficients with the same resolution mentioned in Section 3.1. Therefore, the use of FSK-Gray scheme still does not require changes to the FSCK look-up table

4. Reference state

As mentioned in Section 2.1, radiative properties of gas-soot-particle mixtures in nonhomogeneous media require a single reference state $\boldsymbol{\phi}^0$, derived from which a unified g^0 can be determined for solving Eqs. (12) or (20). Therefore, the choice of $\boldsymbol{\phi}^0$ is very important and should be optimized for any given problem. For a gas-soot mixture at constant total pressure, the reference state is generally evaluated as [24]

$$\boldsymbol{x}^0=\frac{1}{V}\int_V\boldsymbol{x}\mathrm{d}V\tag{21}$$

$$\kappa_{P,0}(T^0,\boldsymbol{x}^0)I_b(T^0)=\frac{1}{V}\int_V\kappa_{P,0}(T_0,\boldsymbol{x})I_b(T_0)\mathrm{d}V\tag{22}$$

where $\boldsymbol{x}$ represents a vector including mole fractions for different gas species and volume fraction for soot. Eqs. (21) and (22) indicate that the reference gas mole fraction and soot volume fraction are volume-averaged and the reference temperature is a Planck-mean temperature based on average emission from gas-soot mixture in the entire volume. This evaluation of reference state was recommended for nonhomogeneous particulate media in [21], in which the results suggested that the choice of reference state was not sensitive to the particle state variables. However, it was found that significant errors may arise if the reference state only considers the gas-soot mixture in nonhomogeneous particulate media. Consequently, a new reference state for nonhomogeneous particulate media is proposed here that employs the same reference gas mole fraction and soot volume fraction as given in Eq. (21), but a different reference temperature evaluated as

$$\begin{aligned}&\kappa_{P,0}(T^0,\mathbf{x}^0)I_b(T^0)+\textstyle\sum_{i=1}^{N}\kappa_{P,i}(T^0,\mathbf{v}_i^0)I_b(T^0)\\&=\frac{1}{V}\int_V\left[\kappa_{P,0}(T_0,\mathbf{x})I_b(T_0)+\textstyle\sum_{i=1}^{N}\kappa_{P,i}(T_i,\mathbf{v}_i)I_b(T_i)\right]\mathrm{d}V\end{aligned}\tag{23}$$

where $\mathbf{v}_i$ represents a vector including particle projected area per unit volume and volume fraction for phase i; $\mathbf{v}_i^0$ can be calculated by the same volume averaged method as used in Eq. (21). Thus, the reference temperature becomes a Planck-mean temperature based on total emission from both gas-soot mixture and particles.

In order to test the quality of these two possible reference temperatures, radiation in a nonhomogeneous gas-particle mixture across a 1D slab bounded by two parallel black cold walls is considered. The gas phase has 10% CO_2 and 90% N_2 at 1000 K. The particles are char at 1500 K with a uniform diameter of 200 μm and volume fraction of 10^{-3}. Other calculation conditions are shown in Table 1. The negative radiative heat sources using different methods are shown in Fig. 2. For all FSK schemes, the reference mole fraction of CO_2 is 0.1. The reference temperature for the FSK-Gray (G) and FSK-FSK (G) schemes is calculated by Eq. (22) which is 1000 K while that for the FSK-Gray (GP) and FSK-FSK

Table 1
Calculation conditions.

RTE solver	P_1	
Reference solution	LBL-LBL scheme	
Gas-soot correlated-k	From the FSCK look-up table	
Particle correlated-k	On-the-fly calculation	
Particle Planck-mean absorption coefficient	On-the-fly calculation	
Particle Planck-mean scattering coefficient	On-the-fly calculation	
Quadrature for FSK calculations	32-point Gauss quadrature	
Complex index of refraction	Char	2.20–1.12i
	Bituminous	1.85–0.22i
	Fly ash	1.50–0.02i

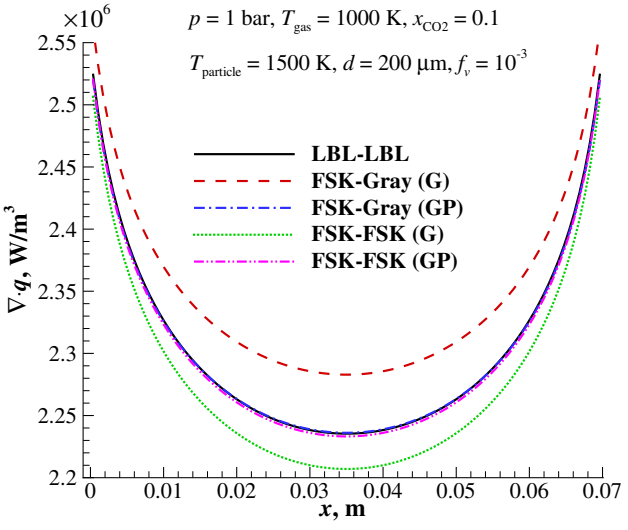

Fig. 2. Comparison of negative radiative heat sources across 1D slab using different methods with reference state of FSK method evaluated using gas phase only (G) or including gas-particulate phase (GP).

(GP) schemes is calculated by Eq. (23) which attains a higher value of 1418 K. The results using the FSK-Gray (G) or the FSK-FSK (G) schemes show large discrepancies, which mainly results from ignoring the particulate phase in the reference state. In contrast, both FSK-Gray (GP) and FSK-FSK (GP) schemes give almost identically good results compared to the LBL-LBL scheme. This illustrates that Eq. (23) is more appropriate for FSK calculations in nonhomogeneous particulate media and is used in this work.

5. Results and discussion

In order to verify the schemes proposed in Section 3, radiative calculations for 1D slabs and a realistic coal flame are carried out, with emission and negative radiative heat source $\nabla \cdot q$ predicted using both the FSK-FSK scheme and the FSK-Gray scheme. Total pressure is 1 bar and other calculation conditions can be found in Table 1.

5.1. Sample calculations

To demonstrate the accuracy of the schemes in nonhomogeneous gas-particle fields 1D slabs bounded by two parallel black cold walls are considered. The slabs are geometrically divided into two equal-width layers filled with gas-soot-particle mixtures. For all four test cases, the left layer has a temperature of 1000 K for particles and 1200 K for a gas-soot mixture comprised of 5% CO_2-10% H_2O-10% CO-75% N_2 and a soot volume fraction of 10^{-6}, while the right layer has a temperature of 2000 K for particles and 1800 K for a gas-soot mixture containing 10% CO_2-20% H_2O-5% CO-65% N_2 and a soot volume fraction of 5×10^{-7}. The particles here are char with particle volume fractions and sizes listed in Table 2. Most of these configurations were proposed in [21] to approximate both unburned and burning gas-particle environments in typical pulverized and fluidized-bed coal combustion conditions. For large particle volume fractions, the test layer thicknesses are reduced due to large optical thicknesses.

Figs. 3–6 show distributions of both emission and $\nabla \cdot q$ across the slabs using the FSK-Gray and the FSK-FSK schemes compared against those of benchmark LBL calculations. The correlated k-values of gas-soot mixtures from the FSCK look-up table and those of particles, in principle, preserve the emission term, which is demonstrated by the well overlapped emission terms obtained from the LBL and FSK calculations in these figures.

For all cases, $\nabla \cdot q$ in the left (cold) layer near the interface deviates significantly from the emission spectrum at the local temperature since incident radiation at those locations is dominated by strong emission from the right (hot) layer, where noticeable errors in the FSK calculations may occur. Away from the interface in the cold layer, such deviation is reduced. This phenomenon is barely observed in the hot layer because emission from the cold layer is negligible. Hence, the problem approaches the case of a standalone homogeneous hot layer and the results for $\nabla \cdot q$ in this layer using both schemes are almost error-free compared to benchmark LBL results.

Table 2
Layer width (l), particle diameter (d) and particle volume fraction (f_v) for 1D cases.

Case	Left layer			Right layer		
	l, m	d, μm	f_v	l, m	d, μm	f_v
A	0.05	200	10^{-3}	0.05	100	2.5×10^{-4}
B	0.05	2	10^{-4}	0.05	0.4	10^{-5}
C	0.005	600	0.6	0.005	400	0.05
D	0.005	600	0.3	0.005	400	0.1

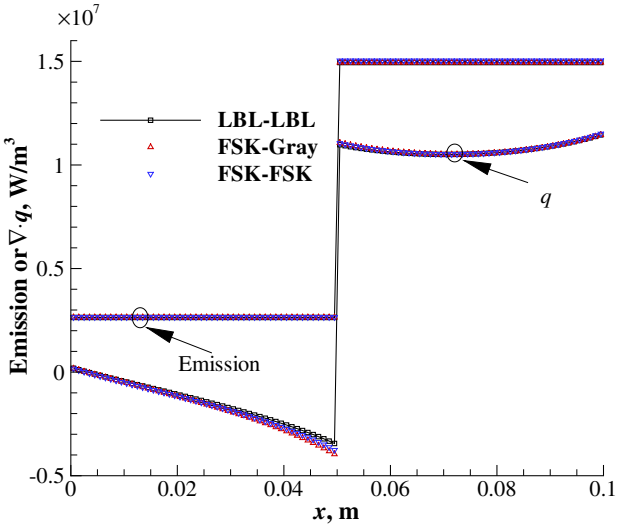

Fig. 3. Comparisons of emission and negative radiative heat source using different methods for Case A.

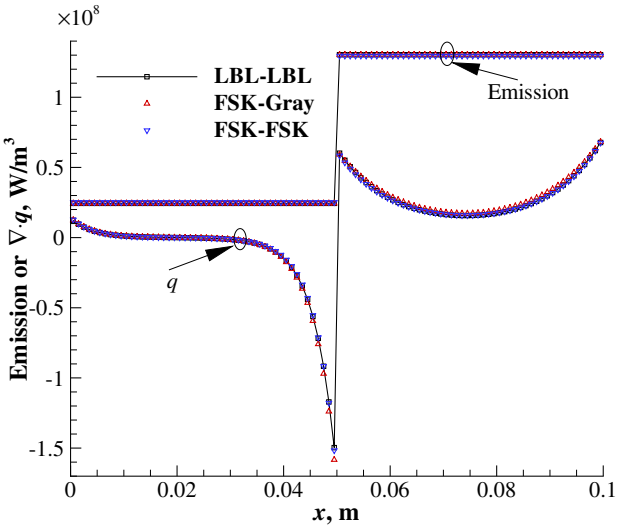

Fig. 4. Comparisons of emission and negative radiative heat source using different methods for Case B.

The noticeable errors for $\nabla \cdot q$ in the cold layer using the FSK-Gray scheme mainly come from the employment of the correlation principle for gas-soot mixtures and ignoring spectral behavior for particles while those using the FSK-FSK scheme are due only to the employment of the correlation principle for both gas and particulate phases. From Figs. 3 to 6, it can be observed near the center of slab that the departures from LBL calculations using the FSK-Gray scheme are relatively larger than those using the FSK-FSK scheme. For pulverized coal cases, Cases A and B, shown in Figs. 3 and 4, the results using the FSK-FSK scheme almost fully overlap with the benchmark results, illustrating that errors from the employment of the correlation principle can be ignored. This also means the errors using the FSK-Gray scheme stem mainly from ignoring the spectral behavior of particles, but the increase in error is minimal. For fluidized-bed coal cases, Cases C and D, shown in Figs. 5 and 6, emission from particles dominates because of the significantly increased particulate volume fraction, for which the effects of ignoring spectral behavior for particles on the accuracy become a little more severe. However, the FSK-Gray scheme still

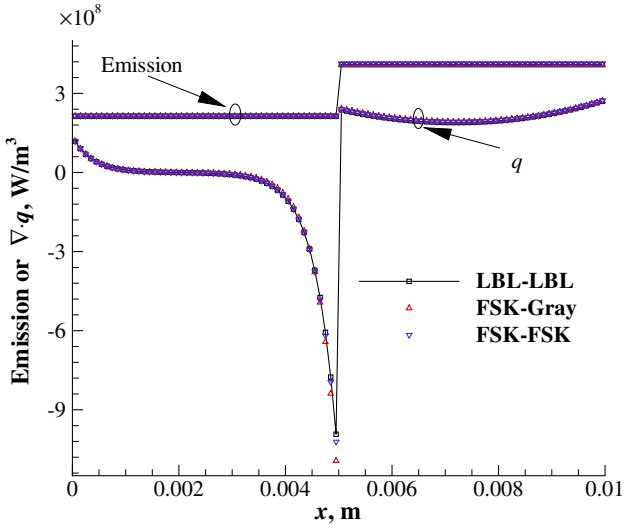

Fig. 5. Comparisons of emission and negative radiative heat source using different methods for Case C.

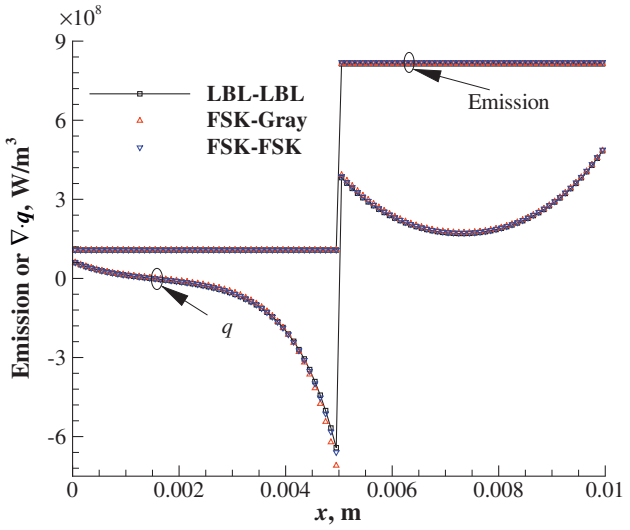

Fig. 6. Comparisons of emission and negative radiative heat source using different methods for Case D.

accurately predicts the trends of $\nabla\cdot q$. While small errors due to employment of the correlation principle or/and ignoring spectral behavior of particles remain, both FSK schemes give excellent predictions of radiative heat sources in nonhomogeneous particulate media.

To test the efficiency, CPU times for generating particle absorption coefficients used in the LBL-LBL calculations, the particle correlated k-values used in the FSK-FSK schemes and the particle Planck-mean absorption coefficients used in the FSK-Gray scheme at arbitrary thermodynamic states are compared. The pressure is fixed at 1 bar and the temperature range for arbitrary thermodynamic states is from 300 K to 3000 K. Particles with volume fractions ranging from 0 to 0.6 and diameters ranging from 1 μm to 500 μm are included in the generation. In the LBL-LBL calculations, the resolution of absorption coefficients is set to 0.01 cm^{-1} in order to trace all possible spectral complexities in the gas phase; while in FSK calculations for particles, 100 cm^{-1} is verified to be able to give error-free Planck-mean absorption coefficients compared to that calculated by the absorption coefficients with high resolution. As expected, the CPU cost for LBL calculations is largest as shown in Table 3. Due to the assembly of two k-distributions as well as the interpolation process, the CPU time for the FSK-FSK scheme is larger than that for the FSK-Gray scheme. During radiative calculations, generating particle k-distributions only consumes a small portion of total CPU time and, therefore, the increment of CPU cost for the FSK-FSK scheme should be acceptable in practical applications, as demonstrated in the following section.

5.2. Flame calculations

To further test accuracy as well as efficiency of the FSK-FSK scheme, radiative heat transfer for a realistic coal flame is calculated. The target configuration is a laboratory-scale pulverized-coal flame with the central air jet entraining bituminous coal particles into the hot flue gas [29]. This flame has been studied in a wide range of coal combustion focusing on ignition and pyrolysis characteristics [30], turbulence models [31], chemistry [32] and radiation effects [2]. To model this coal flame, a Eulerian-Lagrangian method implemented in OpenFOAM-2.3.x is used with the carrier gas modeled by Eulerian equations and the particles tracked in a Lagrangian framework. The computational mesh employed in this work is a 10° axisymmetric wedge consisting of 15,000 hexahedral cells with a single cell thick in the azimuthal direction. For gas phase combustion, a systematically reduced methane mechanism [32] is used to model the kinetics. Other physical models and numerical algorithms used here are the same as those used in [2]. It should be noted that the purpose of this modelling is not to resolve the flame details quantitatively with sophisticated turbulence and combustion models, but to demonstrate the validity of both the FSK-Gray and the FSK-FSK schemes in a realistic flame. Hence, only quasi-steady time-average profiles shown in Fig. 7 are used for radiative calculation comparisons, i.e., turbulence-radiation interaction is not considered.

To determine the radiative heat sources for the Eulerian mesh, radiative properties of the Lagrangian particles are required for each cell. Assuming a number of J particles to be located in cell i, the cell-based volume fraction $f_{v,C}$ and the projected area per unit volume $f_{A,C}$ are expressed as

$$f_{v,C} = \sum_{j=1}^{J} f_{v,j} \tag{24}$$

$$f_{A,C} = \sum_{j=1}^{J} f_{A,j} \tag{25}$$

With cell-based projected area per unit volume, the cell-based particle temperature T_c can be calculated in a manner that conserves emission of particles located in the same cell, i.e.,

$$\kappa^* f_{A,C}\sigma T_C^4 = \sum_{j=1}^{J} \kappa^* f_{A,j}\sigma T_j^4 \tag{26}$$

which gives

$$T_c = \sqrt[4]{\frac{\sum_{j=1}^{J} f_{A,j} T_j^4}{f_{A,C}}} \tag{27}$$

Table 3
CPU time comparisons of generating spectral properties for particles at 100 thermodynamic states based on different schemes.

Scheme	CPU (s)
LBL-LBL	46.25
FSK-Gray	0.005
FSK-FSK	0.06

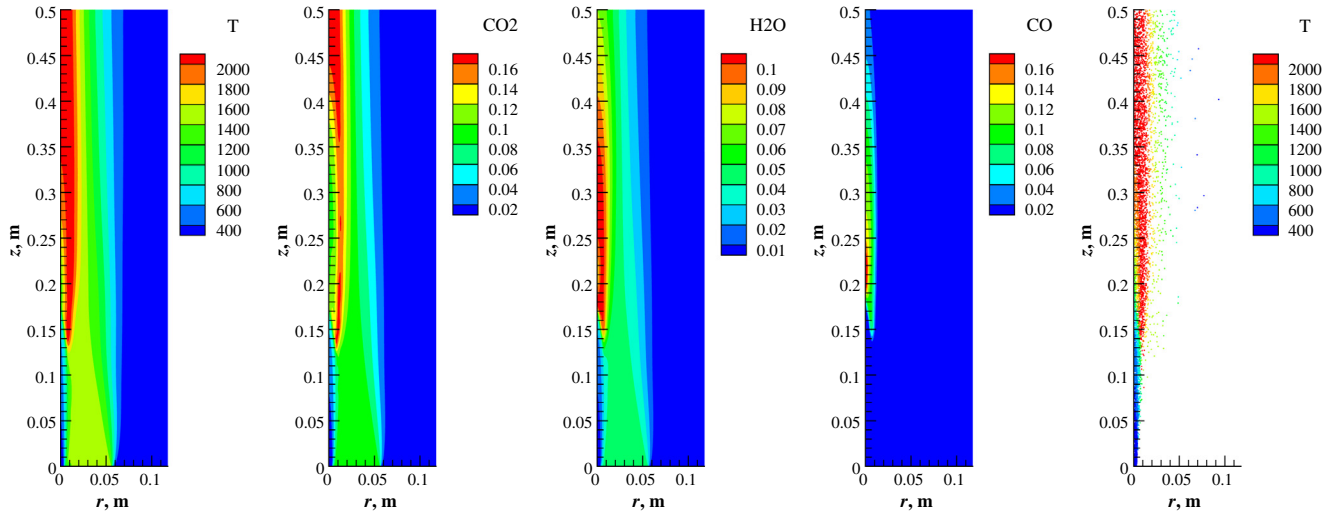

Fig. 7. Time-averaged spatial profile of gas phase temperature, CO_2 mass fraction, H_2O mass fraction, CO mass fraction and distribution of particles colored by their temperatures.

where κ^* is the nondimensional absorption coefficient calculated by the Buckius and Hwang correlations [19], which depends on the complex index of refraction and a mean particle diameter determined by $f_{v,C}$ and $f_{A,C}$. During combustion particles composed of pristine coal or ash rarely exist; most coal particles are partially burnt, especially for the laboratory-scale pulverized coal flame studied here. Therefore, a model to calculate the complex index of refraction of partially burnt coal particles is needed. Here, a binary-switch model is used, where the complex index of refraction is switched to that of the fly ash when only 5% of the cell-based initial mass of the solid carbon remains.

Employing the cell-based radiative properties of particles together with those of gases, volumetric emission and the negative radiative heat source, $\nabla \cdot q$, are determined using both the FSK-Gray and the FSK-FSK schemes without feedback to the flame. The LBL-LBL calculations provide a reference solution. Fig. 8 gives the results for both volumetric emission and $\nabla \cdot q$ as well as the distribution of state variables at two axial locations. During combustion, the Lagrangian particles are discretely distributed across the domain as shown in the right most part of Fig. 7, indicating that some cells may be filled with a large number of particles while others are not or even without particles. This explains why the cell-based volumetric emission and $\nabla \cdot q$ show oscillating behavior at the locations where particles exist.

At $z = 0.05$ m, the coal particles have not ignited and are still being heated by the hot gases. While the temperatures of particles are lower than those of the gas phase, emission from particles is appreciable as compared to that from the hot gas. This is because the large cell-based projected area per unit volume as shown in Fig. 8a results in large absorption coefficients for particles. Near the axis at $z = 0.05$ m where there is strong self-absorption, the FSK-Gray scheme gives relatively large errors for the prediction of $\nabla \cdot q$ due to the gray assumption for particles. Even the FSK-FSK scheme incurs some errors close to the axis. The reason is that the correlation principle for particles is greatly challenged in low temperature environments, for which the radiative contributions can be neglected. At most locations across $z = 0.05$ m (Fig. 8b), both the FSK-Gray and FSK-FSK schemes give excellent predictions of the radiative heat source compared to the benchmark LBL calculations.

As seen from Fig. 7, the coal particles are ignited at approximately $z = 0.13$ m, downstream of which a continuous flame begins to develop. It is indispensable to test the FSK-FSK scheme in these regions and the location of $z = 0.25$ m is chosen in this work as a representative example as shown in Fig. 8c and d. Since char oxidation produces additional heat along the flame front, the particle temperature at $z = 0.25$ m has a maximum of 500 K above that of surrounding gas; correspondingly, most of the emission is from particles. However, due to the small size of this coal flame, self-absorption of particles tends to be near zero such that $\nabla \cdot q$ almost overlaps with emission. The same phenomenon is found at other axial locations where the coal particles are burning. While it is hard to test the accuracy of the FSK schemes at $z = 0.25$ m for the prediction of $\nabla \cdot q$, the overlapped emission using different schemes still illustrate that both FSK schemes can be applied to laboratory-scale coal flames.

Since optical thicknesses in boilers with coal combustion are generally very large, it is expected to test the FSK-FSK scheme in cases where self-absorption of particles is significant. This is achieved by enlarging the original coal flame shown in Fig. 7 with mesh size in each direction increased by a factor of 20. Similarly, the same scaling is applied to the particles' coordinates and other parameters remain unchanged. Radiative heat transfer is recalculated using the different schemes and the results at $z = 5$ m (scaling from $z = 0.25$ m by a factor of 20) are shown in Fig. 9. Since state variables are unchanged, emission shown in Fig. 9 is exactly the same as in Fig. 8d. With the increased optical thicknesses, particles absorb a large amount of emission, especially at locations close to the axis. It can be seen from Fig. 9 that the results of $\nabla \cdot q$ using both the FSK-Gray and the FSK-FSK schemes overlap very well with the reference LBL calculations at most locations along the radial direction, which illustrates that treating particles as gray is definitely valid for practical applications. Thus, both the FSK-Gray and the FSK-FSK schemes are the safe choices to predict radiative heat sources for realistic flames with one particulate phase.

Moreover, to test the performance of both schemes in multi-phase particulate media, the scaled case shown in Fig. 9 is recalculated by treating the coal as two separate particulate phases, i.e., unburned char and fly ash. For each particulate phase, the cell-based volume fraction and projected area per unit volume are calculated based on their own mass fractions. The complex indices of refraction for char and fly ash can be found in Table 1. Other calculation conditions remain the same as those used in Fig. 9. Because of different treatment of coal particles, the LBL-LBL scheme for two particulate phases gives different results compared to that for one particulate phase as shown in Fig. 10a. Results using the two FSK

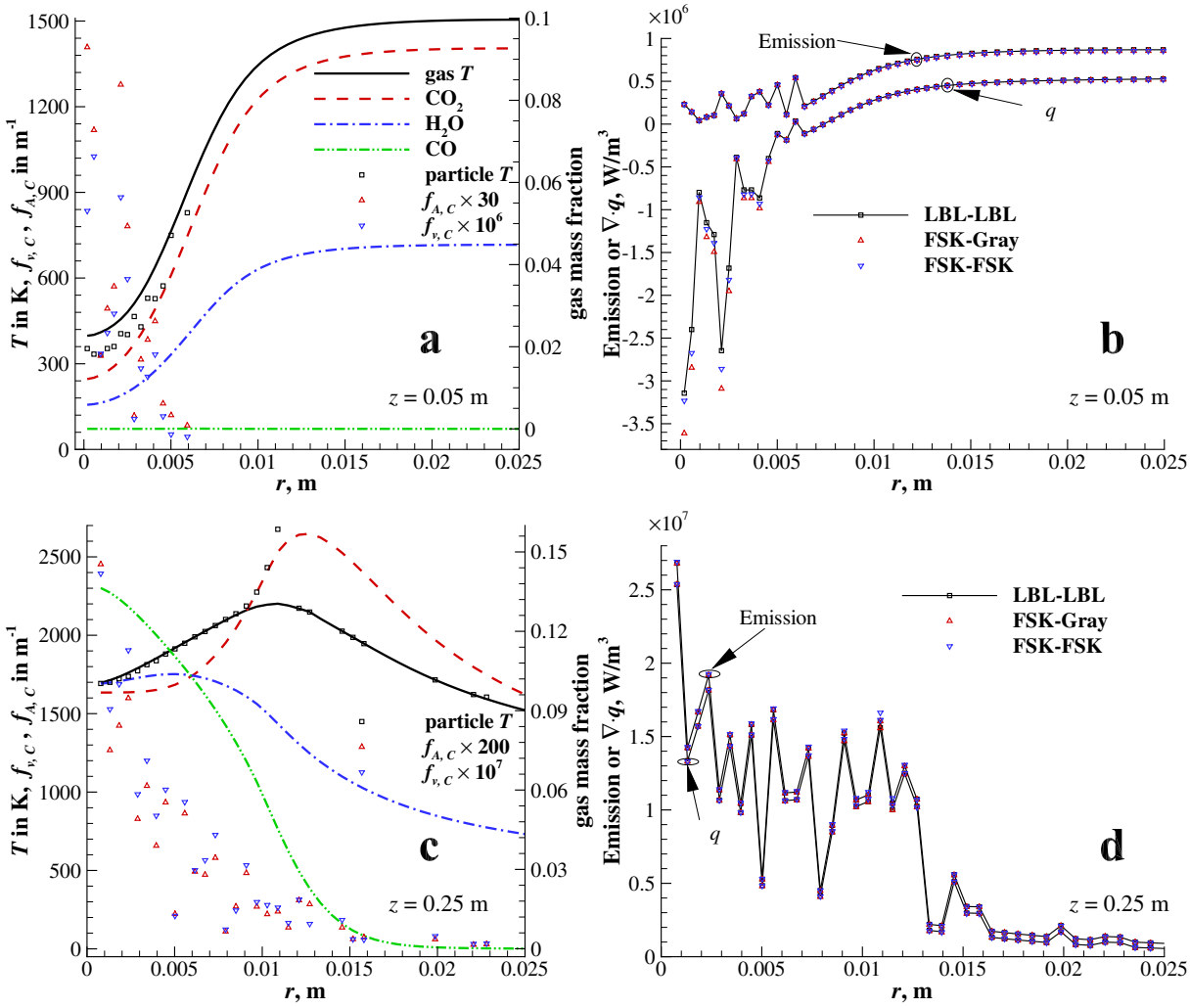

Fig. 8. Comparison of volumetric emission and negative radiative heat source using different methods (right column) for a given field of state variables (left column) at two locations, $z = 0.05$ m (top) and $z = 0.25$ m (bottom); in c, the legends for gas properties are the same as in a (omitted due to limited space).

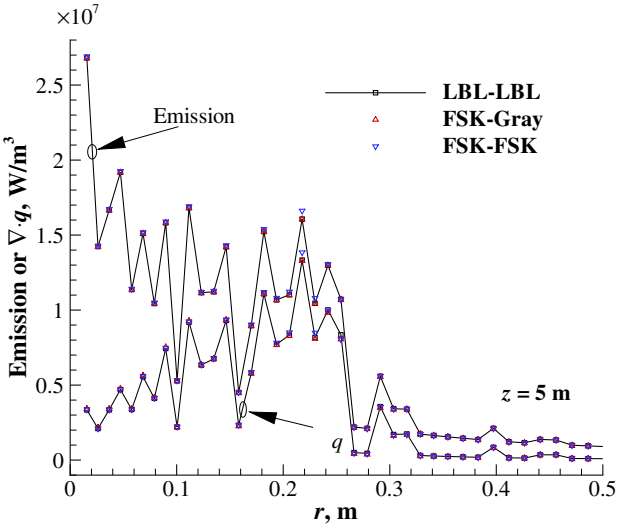

Fig. 9. Volumetric emission and negative radiative heat source for the scaled coal flame at $z = 5$ m.

schemes for the two-phase case are also included in Fig. 10b, in which all FSK calculations show excellent agreement with the benchmark LBL-LBL results. This demonstrates that both FSK-Gray and FSK-FSK schemes can be applied to multiphase particulate media.

CPU times using different schemes for the scaled coal flame are compared in Table 4. Because of approximately one million evaluations of the RTE, the LBL-LBL calculations for both 1 phase and 2 phases require a large amount of CPU time; the double calculations of one million particle absorption coefficients for 2 phases increases CPU significantly. For calculations using both FSK schemes, only 32 RTE evaluations are employed here, leading to considerable savings in CPU time. A 32-point quadrature scheme was chosen to assure negligible quadrature errors, while 8 points should suffice in most practical applications. While generation of particle k-distributions for the FSK-FSK scheme consumes additional CPU time as shown in Table 3, the difference in CPU cost for flame calculations between the FSK-Gray scheme and the FSK-FSK scheme is minor. The reason is that the CPU time used for calculations of particle spectral properties is tiny and most of the CPU time is used for gas k-distribution generations and RTE evaluations. This also explains the reason why increasing the number of particulate phases incurs only minor additional CPU cost for both FSK schemes. Therefore, the FSK-Gray scheme and the FSK-FSK scheme can be treated to be equally efficient for realistic applications. Together with the accuracy discussions above, both the FSK-Gray and FSK-FSK schemes are appropriate for use in nonhomogeneous particulate media.

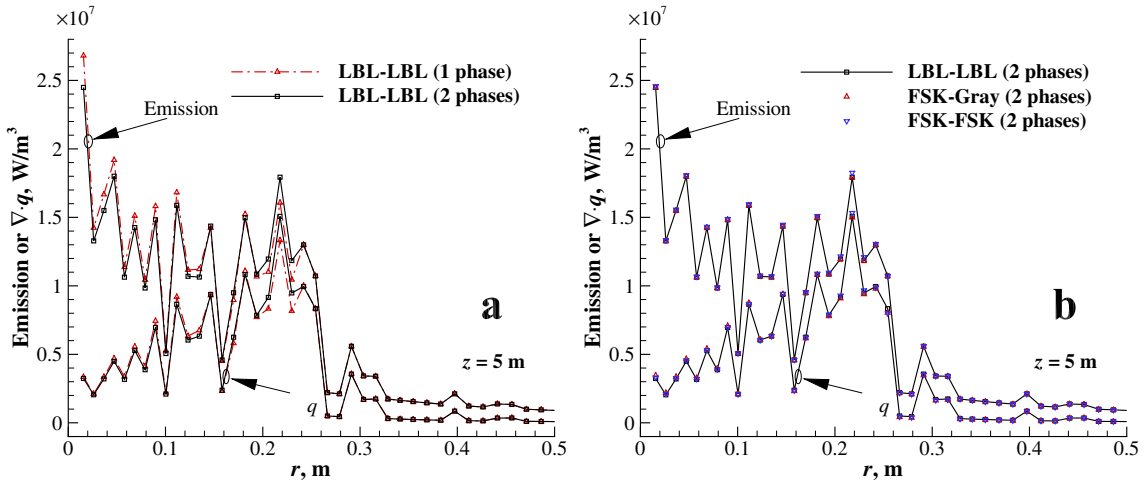

Fig. 10. Volumetric emission and negative radiative heat source for the scaled coal flame at $z = 5$ m; (a) comparison of benchmark LBL-LBL solution for different treatment of coal particles, (b) comparison of different methods for two-phase case.

Table 4
CPU time comparisons of radiative calculations for the scaled coal flame case using different schemes.

Scheme	Number of particulate phase	CPU (s)
LBL-LBL	1	0.72×10^6
	2	1.09×10^6
FSK-Gray	1	4.95
	2	5.21
FSK-FSK	1	5.35
	2	5.87

6. Conclusions

In this work, two schemes, i.e., gas FSK-particle FSK (FSK-FSK) and gas FSK-particle Gray (FSK-Gray) schemes were developed for the treatment of nongray spectral properties in nonhomogeneous multi-phase media with individual temperatures for each phase. The FSK-FSK scheme employs the correlation principle to combine correlated k-values of gas-soot mixtures from an FSCK look-up table with those of particles calculated on-the-fly, while the FSK-Gray scheme treats particles as gray and directly employs the Planck-mean absorption coefficients of particles for radiative calculations. Since the spectral properties for particles are calculated on-the-fly, use of either scheme does not require any changes to the FSCK look-up table nor increases its size. Both accuracy and efficiency were verified for the two schemes using several sample calculations and a realistic coal flame simulation.

While most test cases in this work involve only two solid phases, the theoretical derivation of both FSK schemes was presented for an arbitrary number of solid phases. This is indicated by the subscript i in those derivations and the scenarios for multiple solid phases are the same as those for a single solid phase. Employment of the correlation principle and ignoring the spectral behavior of particles may result in some errors, which were shown to be negligible in high temperature environments. CPU time increases as the number of particulate phases increases; however, the increment is minimal. Therefore, both FSK schemes extend the applications for the FSCK look-up table from gas-soot mixtures with a single temperature to the case of multi-phase mixtures with individual temperatures for each phase.

For all cases tested here the FSK-Gray scheme provided sufficiently accurate results. However, the FSK-FSK scheme includes more detailed spectral consideration for particles and, therefore, is able to simulate particle radiation more accurately than the FSK-Gray scheme. Since CPU requirements for both FSK schemes are roughly the same, the use of the FSK-FSK scheme is recommended.

Acknowledgments

This work was financially supported by “the Fundamental Research Funds for the Central Universities”, Grant No. 2018JBM047, “the National Key R&D Program of China”, Grant No. 2017YFB0602003 and “the National Natural Science Foundation of China”, Grant No. 51576014.

References

[1] X. Yang, A. Clements, J. Szuhánszki, X.H. Huang, O.F. Moguel, J. Li, et al., Prediction of the radiative heat transfer in small and large scale oxy-coal furnaces, Appl. Energy 211 (2018) 523–537.
[2] B.F. Wu, S.P. Roy, X.Y. Zhao, M.F. Modest, Effect of multiphase radiation on coal combustion in a pulverized coal jet flame, J. Quant. Spectrosc. Radiat. Transfer 197 (2017) 154–165.
[3] J. Cai, M. Handa, M.F. Modest, Eulerian-Eulerian multi-fluid methods for pulverized coal flames with nongray radiation, Combust. Flame 162 (2015) 1550–1565.
[4] C. Ates, N. Selçuk, G. Kulah, Significance of particle concentration distribution on radiative heat transfer in circulating fluidized bed combustors, Int. J. Heat Mass Transf. 117 (2018) 58–70.
[5] D.E. Alagoz, G. Kulah, N. Selçuk, A comprehensive fluidized bed combustion model coupled with a radiation model, Combust. Sci. Technol. 180 (2008) 910–926.
[6] Y. Hua, G. Flamant, J. Lu, D. Gauthier, 3D modelling of radiative heat transfer in circulating fluidized bed combustors: influence of the particulate composition, Int. J. Heat Mass Transf. 48 (2005) 1145–1154.
[7] M. Eriksson, M.R. Golriz, Radiation heat transfer in circulating fluidized bed combustors, Int. J. Therm. Sci. 44 (4) (2005) 399–409.
[8] M.F. Modest, The treatment of nongray properties in radiative heat transfer: from past to present, ASME J. Heat Transf. 135 (2013) 061801-1–061801-12.
[9] H.Q. Chu, F. Ren, Y. Feng, M.Y. Gu, S. Zheng, A comprehensive evaluation of the non gray gas thermal radiation using the line-by-line model in one- and two-dimensional enclosures, Appl. Therm. Eng. 124 (2017) 362–370.
[10] J.O. Arnold, E.E. Whiting, G.C. Lyle, Line-by-line calculation of spectra from diatomic molecules and atoms assuming a voigt line profile, J. Quant. Spectrosc. Radiat. Transfer 9 (6) (1969) 775–798.
[11] M.F. Modest, Narrow-band and full-spectrum k-distributions for radiative heat transfer-correlated-k vs. scaling approximation, J. Quant. Spectrosc. Radiat. Transfer 76 (1) (2003) 69–83.
[12] C.J. Wang, W.J. Ge, M.F. Modest, B.S. He, A full-spectrum k-distribution look-up table for radiative transfer in nonhomogeneous gaseous media, J. Quant. Spectrosc. Radiat. Transfer 168 (2016) 46–56.
[13] V.P. Solovjov, B.W. Webb, An efficient method for modeling radiative transfer in multicomponent gas mixtures with soot, ASME J. Heat Transf. 123 (2001) 450–457.

[14] M.K. Denison, B.W. Webb, k-Distributions and weighted-sum-of-gray-gases–A hybrid model, Int. Heat Transfer Conf. 2 (1994) 19–24.
[15] H. Chang, T.T. Charalampopoulos, Determination of the wavelength dependence of refractive indices of flame soot, Proc. Roy. Soc. London (1990) 577–591.
[16] C.J. Wang, M.F. Modest, B.S. He, Full-spectrum *k*-distribution look-up table for nonhomogeneous gas–soot mixtures, J. Quant. Spectrosc. Radiat. Transfer 176 (2016) 129–136.
[17] C.J. Wang, M.F. Modest, B.S. He, Improvement of full-spectrum *k*-distribution method using quadrature transformation, Int. J. Therm. Sci. 108 (2016) 100–107.
[18] C.J. Wang, M.F. Modest, B.S. He, Efficient full-spectrum correlated-*k*-distribution look-up table, J. Quant. Spectrosc. Radiat. Transfer 219 (2018) 108–116.
[19] R.O. Buckius, D.C. Hwang, Radiation Properties for polydispersions: application to Coal, ASME J. Heat Transf. 102 (1980) 99–103.
[20] M.P. Mengüç, R. Viskanta, On the radiative properties of polydispersions: a simplified approach, Combust. Sci. Technol. 44 (1985) 143–159.
[21] J. Cai, M.F. Modest, Absorption coefficient regression scheme for splitting radiative heat sources across phases in gas-particulate mixtures, Powder Technol. 265 (2014) 76–82.
[22] J.J. Guo, F. Hu, W. Luo, P.F. Li, Z.H. Liu, A full spectrum *k*-distribution based non-gray radiative property model for fly ash particles, Int. J. Heat Mass Transf. 118 (2018) 103–115.
[23] J.J. Guo, F. Hu, W. Luo, P.F. Li, Z.H. Liu, A full spectrum *k*-distribution based non-gray radiative property model for unburnt char, Proc. Combust. Inst. 37 (2019) 3081–3089.
[24] M.F. Modest, Radiative Heat Transfer, third ed., Academic Press, New York, 2013.
[25] M.F. Modest, R.J. Riazzi, Assembly of full-spectrum *k*-distributions from a narrow-band database: effects of mixing gases, gases and nongray absorbing particles, and mixtures with nongray scatterers in nongray enclosures, J. Quant. Spectrosc. Radiat. Transfer 90 (2) (2005) 169–189.
[26] A.Q. Wang, Investigation of Turbulence-Radiation Interaction in Turbulent Flames Using a Hybrid Finite Volume/Monte Carlo approach PhD thesis, Pennsylvania State University, Pennsylvania, 2007.
[27] L.S. Rothman, I.E. Gordon, R.J. Barber, H. Dothe, R.R. Gamache, A. Goldman, et al., HITEMP, the high-temperature molecular spectroscopic database, J. Quant. Spectrosc. Radiat. Transfer 111 (15) (2010) 2139–2150.
[28] V.P. Solovjov, B.W. Webb, SLW modeling of radiative transfer in multicomponent gas mixtures, J. Quant. Spectrosc. Radiat. Transfer 65 (2000) 655–672.
[29] M. Taniguchi, H. Okazaki, H. Kobayashi, S. Azuhata, H. Miyadera, H. Muto, et al., Pyrolysis and ignition characteristics of pulverized coal particles, ASME J. Energy Resour. Technol. 123 (2001) 32–38.
[30] K. Yamamoto, T. Murota, T. Okazaki, M. Taniguchi, Large eddy simulation of a pulverized coal jet flame ignited by a preheated gas flow, Proc. Combust. Inst. 33 (2011) 1771–1778.
[31] X.Y. Zhao, D.C. Haworth, Transported PDF modeling of pulverized coal jet flames, Combust. Flame 161 (2014) 1866–1882.
[32] S.M. Correa, M.E. Braaten, Parallel simulations of partially stirred methane combustion, Combust. Flame 94 (1993) 469–486.